BJRS

BRAZILIAN JOURNAL
OF
RADIATION SCIENCES
11-01A (2023) | 01-31 | e2151

Determination of steel and lead bi-laminated shielding for military vehicles

Azevedo[a], A. M.; Cardoso[a], D.O.; Medeiros[a], M.P.C.; Gavazza[a], S.; Morales[a], R. K.

[a]*Instituto Militar de Engenharia / Seção de Engenharia Nuclear (SE/7). Praça General Tibúrcio, 80, 22290-270, Urca, Rio de Janeiro, RJ, Brasil.*

ary.azevedo92@gmail.com

ABSTRACT

In the present work, the transmission factors of γ-rays are determined in bi-layered shields composed of lead and steel, through a methodology composed of three distinct parts. The buildup calculation was performed using the methodology published by Broder in 1962 [1]. A computational simulation was used through a spherical model, a total of three concentric spheres were simulated, with the source in the center of the spheres. The first sphere represents the lead shield and its radius is represented by the thickness of this material. The second sphere represents the steel shield and its radius is the sum of the thicknesses of the shielding. The third sphere is the vacuum that will determine the number of photons that will pass. To verify if the analytical methodology can be used to calculate the transmission factor of the proposed shield, laboratory experiments were performed with the BGO (Bismuth Germanate) detector. Measurements were only made with the thickness of steel, and with 15 different thicknesses of lead, ranging from 0.11 cm to 2.01 cm, while keeping the steel thickness. Three different thicknesses of steel were used: 0.65 cm, 0.85 cm and 1.40 cm. The work is relevant in the field of radiological and nuclear defense, considering the application of this shield in military vehicles, and the efficiency of the proposed analytical methodology was demonstrated.

Keywords: **Vehicle CBRN. Shielding of gamma-ray. Factor transmission. Bilaminated shielding. MCNP.**

ISSN: 2319-0612
DOI: https://doi.org/10.15392/2319-0612.2023.2151
Submitted: 2022-11-10
Accepted: 2023-04-28

1. INTRODUCTION

Over time, several accidents have occurred, one of the most well-known and considered the worst nuclear accident in history was the one that occurred on April 26th, 1986 in Chernobyl. In short, after a system failure, the reactor core exploded, generating a nuclear plume into the atmosphere. [2]

In Brazil, in September 1987, there was a radiological accident in Goiânia, where a source of Cesium 137 from a radiotherapy device located at the Goiano Institute of Radiotherapy caused the accident. The sealed source of Cesium 137, which was surrounded by a lead and concrete enclosure, was ruptured, and contamination occurred due to the handling of the material and the dispersion of the aerosol generated during the breach of the source. [3]

In addition to potential accidents, terrorist groups make use of radiological material using RDD - Radiological Dispersion Device - also known as a dirty bomb, which can generally be characterized as the dispersion of radioactive material through explosives. [4]

A Brazilian company in 1980 began the development of a prototype combat vehicle, the *EE-T1 Osório*, which can be seen in Figure 1, to meet the demands of Saudi Arabia. The prototype in question, in its tests, had better results than the French, British, and North American *M1-Abrams* armored vehicles.[5]

One of the versions of this vehicle would be for Chemical, Biological, Radiological, and Nuclear Defense (CBRND) and could operate in radiologically contaminated scenarios. As the developing company declared bankruptcy, the project was discontinued.[5]

Figure 1: *Tank EE-T1 Osorio.*

Source: ANGELS et al 2019. [5]

The objective of this work is to prove that the proposed analytical method can be used for the design of bi-laminated shields made of steel and lead.

The work will compare the results obtained through simulation and laboratory experiments with the sequence of analytical calculations that have already been developed by SE/7, the Nuclear Engineering section, for multilayered shielding.

In this context, the possibility of dimensioning the armor of the vehicles available to the Brazilian Army to use them in the rescue of individuals in emergency scenarios without causing biological damage to the crew is envisioned.

2. MATERIALS AND METHODS

The following materials were used for the development of the work: steel with thicknesses of 1.4 cm, 0.85 cm, and 0.65 cm, supplied by the Army Manufacturing Directorate; 15 lead thicknesses ranging from 0.11 cm to 2.01 cm, provided by the LDIN - Nuclear Instrumentation Laboratory - of the SE/7.

Three methodologies were adopted to achieve the goal of the work: Analytical Methodology, Simulated Methodology, and Experimental Methodology.

It was verified that the chemical composition of the steel contains at least 95% of iron, according to ABNT (Brazilian Association of Technical Standards) and ANSI (American National Standards Institute) standards. Therefore, in the analytical and simulated methodologies, the iron coefficients for steel were considered. [6]

The methodologies were applied only for the energies of Cesium 137, 0.662 MeV, and Cobalt 60, 1.17 MeV and 1.33 MeV. [7]

2.1. Analytical Methodology

The analytical transmission factor was calculated by equation 1, proposed by Broder. [1]

$$FT(i_a + i_c) = A.E(i_a + i_c)\ x\ B_b(i_a + i_c) \qquad (1)$$

In equation 1, $FT(l_a + l_c)$ represents the transmission factor proposed by Broder for two layers. Analytical exponential attenuation for two layers is described by the term A.E.(la + lc). The

analytical buildup is represented by the term B_b(la + lc).The terms I_a and I_c, are free middle paths respectively of steel and lead. These parameters were calculated using equations 2 and 3.

$$i_c = \mu' x' \tag{2}$$

$$i_a = \mu x \tag{3}$$

The linear attenuation coefficients (μ) for iron for the proposed energies are described in Table 1. The data was obtained from NIST-National Institute of Standards and Technology. [8]

Table 1: Interpolated Linear Attenuation Coefficient

Energy (MeV)	**Steel (cm^{-1})**	**Lead (cm^{-1})**
0.662	$5.8x10^{-1}$	1.3
1.17	$4.4x10^{-1}$	$7.3x10^{-1}$
1.33	$3.9x10^{-1}$	$6.2x10^{-1}$

The analytical exponential attenuation for two layers was calculated using equation 4, as proposed by *Broder*. [7]

$$A.E(i_a + i_c) = e^{-(i_a + i_c)} \tag{4}$$

The methodology proposed by Broder for the calculation of the analytical buildup factor was developed. The parameter was calculated using equation 5. [9]

$$B_b(i_a + i_c) = B_{tc}(i_c) + B_{ta}(i_a + i_c) - B_{ta}(i_c) \tag{5}$$

The buildup factors were calculated using the empirical formula of Taylor, as shown in equations 6, 7, and 8. [9]

$$B_{tc}(i_c) = \sum_{n=1}^{2} A'_n e^{-(\alpha'_n i_c)} \quad (6)$$

$$B_{ta}(i_a + i_c) = \sum_{n=1}^{2} A_n e^{-\alpha_n (i_c + i_a)} \quad (7)$$

$$B_{ta}(i_c) = \sum_{n=1}^{2} A_n e^{-(\alpha_n i_c)} \quad (8)$$

The parameters A'_n and α'_n are coefficients for lead, while An and α_n refer to steel. However, at this stage, only those for iron were considered. These are the Taylor parameters, they are constants and tabulated, and can be found in Foderaro's book on shielding [10]. These iron and lead parameters are presented in Tables 2 and 3, respectively.

Table 2: Interpolated Taylor's parameters from lead

Energy (MeV)	$\boldsymbol{A'_1}$	$\boldsymbol{\alpha'_1}$	$\boldsymbol{A'_2}$	$\boldsymbol{\alpha'_2}$
0.662	2.10	-0.032	-1.1	0.253
1.17	3.40	-0.035	-2.4	0.119
1.33	3.80	-0.035	-2.9	0.105

Table 3: Interpolated Taylor's parameters from iron

Energy (MeV)	$\boldsymbol{A_1}$	$\boldsymbol{\alpha_1}$	$\boldsymbol{A_2}$	$\boldsymbol{\alpha_2}$
0.662	29.30	-0.066	-28.30	-0.003
1.17	23.71	-0.058	-22.71	-0.021
1.33	22.54	-0.056	-21.54	0.018

2.2. Simulated Methodology.

In *MCNP5*, a spherical arrangement was simulated, whose main advantage is that its output response can be interpreted for both the collimated experimental arrangement and the non-collimated experimental geometry.

The arrangement consists of three concentric spheres with a point-like and isotropic source at its center. 100 million sotries (*NPS*) were adopted for better counting statistics.

Equations 9, 10, and 11 refer to the principle used, respectively, for the calculation of simulated transmission factor, simulated exponential attenuation, and simulated buildup factor.[11]

$$F.T. = \ collided\ radiation\ +\ non\ collided\ radiation \qquad (9)$$

$$A.E. = \ Radiation\ not\ collided \qquad (10)$$

$$B = \frac{Radiation\ not\ collided}{Radiation\ not\ collided} \qquad (11)$$

The application of these formulas is possible due to the normalized response provided by *MCNP5* and *Tally F1*.

To normalize the response, the software divides the detected photons in the last sphere by the total number of photons emitted by the source.

The *Tally F1* calculates the number of photons or particles that have passed through the desired surface.

Collision radiation was considered, all photons that arrived at the measurement point with energy lower than that of emission. Un-collided radiation, all photons that arrived with their original emission energy.

Figure 2: *Simulated setup sketch*

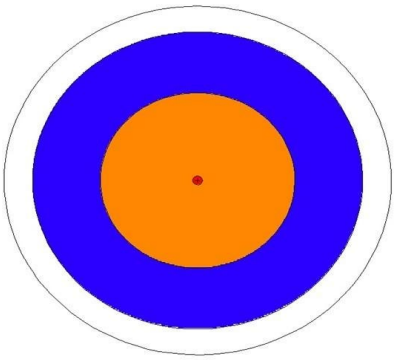

Source: made by the author et al 2022.

2.3. Experimental Methodology in the Laboratory.

Experiments were carried out with the collimated and non-collimated arrangement.

To comparing results, the collimated arrangement is the one in which the buildup factor is equal to 1. In the analytical and simulated methodologies, it is represented by exponential attenuation.

The non-collimated arrangement is referred to when the buildup value is greater than 1. In the analytical and simulated methodology, this value is the transmission factor of the proposed shielding.

The general methodology for obtaining the experimental results was adopted.

1. Bismuth germanate (BGO) detector;

2. Source measurement time:

    Cobalt 60: 150 minutes;

    Cesium 137: 15 minutes.

3. Constant source and distance from the detector;

4. The calculations of the transmission factor were performed with the liquid spectrum;

5. Photopic power channels:

Cesium 137 (0.662 MeV): 1282-1760;

Cobalt 60 (1.17 MeV): 2408-2877;

Cobalt 60 (1.33 MeV): 2878-3165.

The difference in counting time for Cesium 137 and Cobalt 60, considering the counting statistics. An uncertainty of 1% or less was adopted for the methodology. This uncertainty was calculated using equation 12, where 'n' is the number of counts.[12]

$$E = \sqrt{\frac{1}{n}} \tag{12}$$

The difference in counting time for Cesium 137 and Cobalt 60 was due to the activity of Co-60, which has already decayed three half-lives, and Cs-137 has not yet elapsed the first half-life.

The net spectrum was determined by subtracting the background radiation spectrum from the spectrum measured with the source. The background radiation measurement time was the same as that used for the respective sources.

The methodology used to select the photopeak channels of the sources was the window method. A ruler was used to mark the start and end of the counts corresponding to the photopeak. [13]

The materials used in the collimated experimental arrangement: detector shielding, to minimize the energy deposition from background radiation; a collimator (4 mm in diameter) for the radiation source, so that incident photons hit the absorbers at right angles; and shielding for the source to absorb photons not directed at the detector.

The transmission factor for this arrangement was calculated by equation 13.

$$F.T' = \frac{I'}{I'_0} \tag{13}$$

The parameter F.T' represents the transmission factor of the collimated arrangement, I' is the counts made with the steel and lead absorbers (proposed bilaminar shielding for the study) under the photopeak, and I'_0 refers to the counts made without the absorbers under the photopeak.

The result of equation 13 was compared with the analytical and simulated exponential attenuation, as the experimental setup favors the photoelectric effect, since the radiation beam hits the absorber perpendicularly.

Figure 3: *Collimated array*

Figure 4: *Inner part of a collimated array*

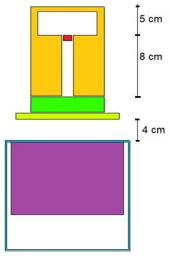

In the sketch presented in Figure 4, the collimator and source shielding are represented in orange, the source in red, the lead absorber in green, the steel absorber in olive green, and the BGO crystal in purple.

The experimental transmission factor was calculated by equation 14. The detector and source shielding, as well as the collimator, were removed to increase the angle of incidence on the steel and lead absorbers.

$$F.T. = \frac{I}{I_0} \tag{14}$$

Figures 5 and 6 represent the experimental arrangement and sketch of the arrangement.

Figure 5: *non-collimated array*

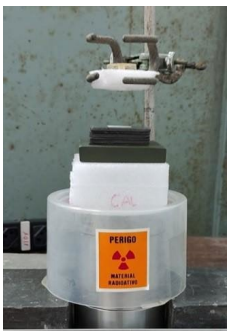

Figure 6: a *sketch of the arrangement*

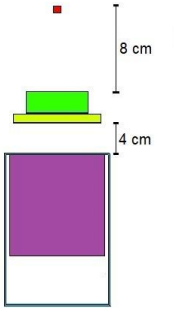

2.4 Experimental methodology in the laboratory

In the analytical methodology adopted, no type of associated error calculation was used.

It was associated with the uncertainties provided by the software (Maestro) to calculate these uncertainties of the experiments. The partial derivatives method was adopted. That when applied we arrived at equations 14, 15 and 16. [12]

$$\sigma(FT') = FT' \sqrt{\left(\frac{\sigma(I\prime)}{I\prime}\right)^2 + \left(\frac{\sigma(I\prime_0)}{I\prime_0}\right)^2} \tag{15}$$

$$\sigma(FT) = FT\sqrt{(\frac{\sigma(I)}{I})^2 + (\frac{\sigma(I_0)}{I_0})^2} \quad (16)$$

$$\sigma(B) = B\sqrt{(\frac{\sigma(A.E.)}{A.E.})^2 + (\frac{\sigma(FT)}{FT})^2} \quad (17)$$

In the simulated methodology, the uncertainties provided by *MCNP5* for the simulated transmission factor and the simulated exponential attenuation were adopted. The error of the simulated buildup was calculated by equation 17.

3. RESULTS

3.1. Experimental Results

The errors associated with the measurements were less than or equal to 0.03.

Table 4: Transmission factor of a collimated array for 0.662 MeV

Lead Thickness (cm)	Transmission factor of good geometry		
	Steel 1.40 cm	**Steel 0.85 cm**	**Steel 0.65 cm**
0.000	0.50	0.67	0.76
0.110	0.44	0.60	0.65
0.180	0.42	0.54	0.62
0.305	0.36	0.43	0.54
0.395	0.29	0.42	0.50
0.530	0.26	0.37	0.42
0.640	0.24	0.33	0.36
0.700	0.22	0.30	0.34
0.805	0.21	0.27	0.31
0.905	0.16	0.23	0.27
1.005	0.14	0.23	0.23
1.200	0.11	0.18	0.19
1.380	0.08	0.13	0.15
1.495	0.08	0.13	0.12
1.675	0.05	0.10	0.07
2.010	0.04	0.07	0.07

Table 5: Transmission factor of a collimated array for 1.17 MeV

Lead Thickness (cm)	Transmission factor of good geometry		
	Steel 1.40 cm	**Steel 0.85 cm**	**Steel 0.65 cm**
0.000	0.57	0.75	0.57
0.110	0.47	0.66	0.74
0.180	0.53	0.66	0.65
0.305	0.51	0.58	0.63
0.395	0.44	0.56	0.67
0.530	0.42	0.57	0.57
0.640	0.39	0.47	0.49
0.700	0.40	0.42	0.54
0.805	0.34	0.47	0.49
0.905	0.32	0.43	0.46
1.005	0.26	0.35	0.38
1.200	0.28	0.36	0.38
1.380	0.21	0.29	0.35
1.495	0.22	0.26	0.29
1.675	0.20	0.22	0.21
2.010	0.14	0.13	0.19

Table 6: Transmission factor of a collimated array for 1.33 MeV

Lead Thickness (cm)	Transmission factor of good geometry		
	Steel 1.40 cm	**Steel 0.85 cm**	**Steel 0.65 cm**
0.000	0.60	0.85	0.60
0.110	0.53	0.77	0.88
0.180	0.54	0.76	0.86
0.305	0.58	0.64	0.76
0.395	0.54	0.66	0.70
0.530	0.45	0.60	0.60
0.640	0.51	0.52	0.56
0.700	0.44	0.47	0.57
0.805	0.37	0.54	0.61
0.905	0.32	0.50	0.56
1.005	0.32	0.44	0.48
1.200	0.38	0.33	0.40
1.380	0.28	0.30	0.37
1.495	0.26	0.28	0.32
1.675	0.23	0.28	0.31
2.010	0.15	0.23	0.27

Table 7: Transmission factor 0.662 MeV

Lead Thickness (cm)	Transmission factor		
	Steel 1.40 cm	**Steel 0.85 cm**	**Steel 0.65 cm**
0.000	0.46	0.61	0.70
0.110	0.41	0.56	0.63
0.180	0.38	0.53	0.58
0.305	0.34	0.48	0.52
0.395	0.31	0.54	0.47
0.530	0.27	0.39	0.42
0.640	0.24	0.36	0.38
0.700	0.22	0.33	0.35
0.805	0.20	0.32	0.35
0.905	0.16	0.28	0.33
1.005	0.16	0.24	0.30
1.200	0.13	0.24	0.24
1.380	0.11	0.23	0.20
1.495	0.09	0.19	0.19
1.675	0.08	0.16	0.17
2.010	0.04	0.12	0.11

3.2. Analytical Results

Table 8: Transmission factor analytical for 0.662 MeV

	Transmission factor		
Lead Thickness (cm)	**Steel 1.40 cm**	**Steel 0.85 cm**	**Steel 0.65 cm**
0.000	0.82	0.92	0.95
0.110	0.73	0.82	0.85
0.180	0.68	0.77	0.80
0.305	0.60	0.68	0.71
0.395	0.54	0.62	0.64
0.530	0.49	0.56	0.58
0.640	0.44	0.50	0.52
0.700	0.40	0.45	0.47
0.805	0.35	0.41	0.42
0.905	0.32	0.37	0.38
1.005	0.28	0.33	0.34
1.200	0.23	0.27	0.28
1.380	0.19	0.22	0.23
1.495	0.17	0.19	0.20
1.675	0.14	0.16	0.16
2.010	0.09	0.11	0.11

Table 9: Transmission factor analysis for 1.17 MeV

Lead Thickness (cm)	Transmission factor		
	Steel 1.40 cm	**Steel 0.85 cm**	**Steel 0.65 cm**
0.000	0.85	0.92	0.95
0.110	0.80	0.87	0.90
0.180	0.77	0.84	0.87
0.305	0.72	0.79	0.81
0.395	0.68	0.75	0.77
0.530	0.65	0.71	0.74
0.640	0.61	0.68	0.70
0.700	0.58	0.64	0.66
0.805	0.55	0.61	0.63
0.905	0.52	0.57	0.59
1.005	0.49	0.54	0.56
1.200	0.44	0.49	0.51
1.380	0.39	0.44	0.46
1.495	0.37	0.41	0.43
1.675	0.33	0.37	0.39
2.010	0.27	0.31	0.32

Table 10: Transmission factor analytical for 1.33 MeV

Lead Thickness (cm)	Transmission factor		
	Steel 1.40 cm	**Steel 0.85 cm**	**Steel 0.65 cm**
0.000	0.86	0.93	0.95
0.110	0.82	0.89	0.91
0.180	0.79	0.86	0.88
0.305	0.75	0.82	0.84
0.395	0.72	0.78	0.80
0.530	0.69	0.75	0.77
0.640	0.66	0.72	0.74
0.700	0.63	0.69	0.71
0.805	0.60	0.66	0.68
0.905	0.58	0.63	0.65
1.005	0.55	0.60	0.62
1.200	0.50	0.55	0.57
1.380	0.46	0.51	0.53
1.495	0.44	0.48	0.50
1.675	0.40	0.44	0.46
2.010	0.34	0.38	0.39

3.3. Simulated Results

The errors associated with the measurements were less than or equal to 0.001.

Table 11: Transmission factor simulated for 0.662 MeV

	Transmission factor		
Lead Thickness (cm)	**Steel 1.40 cm**	**Steel 0.85 cm**	**Steel 0.65 cm**
0.000	0.81	0.91	0.94
0.110	0.80	0.88	0.90
0.180	0.75	0.83	0.85
0.305	0.67	0.74	0.76
0.395	0.61	0.68	0.70
0.530	0.54	0.60	0.62
0.640	0.48	0.54	0.54
0.700	0.46	0.51	0.52
0.805	0.39	0.46	0.47
0.905	0.37	0.42	0.43
1.005	0.34	0.38	0.39
1.200	0.27	0.31	0.32
1.380	0.23	0.26	0.27
1.495	0.20	0.23	0.24
1.675	0.17	0.19	0.20
2.010	0.12	0.13	0.14

Table 12: Transmission factor simulated for 1.17 MeV

Lead Thickness (cm)	Transmission factor		
	Steel 1.40 cm	**Steel 0.85 cm**	**Steel 0.65 cm**
0.000	0.81	0.91	0.94
0.110	0.80	0.88	0.90
0.180	0.75	0.83	0.85
0.305	0.67	0.74	0.76
0.395	0.61	0.68	0.70
0.530	0.54	0.60	0.62
0.640	0.48	0.54	0.54
0.700	0.46	0.51	0.52
0.805	0.39	0.46	0.47
0.905	0.37	0.42	0.43
1.005	0.34	0.38	0.39
1.200	0.27	0.31	0.32
1.380	0.23	0.26	0.27
1.495	0.20	0.23	0.24
1.675	0.17	0.19	0.20
2.010	0.12	0.13	0.14

Table 13: Transmission factor simulated for 1.33 MeV

Lead Thickness (cm)	Transmission factor		
	Steel 1.40 cm	**Steel 0.85 cm**	**Steel 0.65 cm**
0.000	0.94	0.96	0.98
0.110	0.92	0.96	0.97
0.180	0.90	0.94	0.95
0.305	0.86	0.90	0.92
0.395	0.83	0.87	0.89
0.530	0.78	0.83	0.84
0.640	0.75	0.80	0.80
0.700	0.73	0.78	0.79
0.805	0.70	0.75	0.76
0.905	0.67	0.72	0.73
1.005	0.64	0.69	0.70
1.200	0.59	0.63	0.64
1.380	0.54	0.54	0.60
1.495	0.41	0.52	0.57
1.675	0.48	0.51	0.52
2.010	0.41	0.44	0.45

4. ANALYSIS OF RESULTS

4.1 Experimental analysis

The data presented in Figures 7, 8 and 9 show the results of the transmission factor of the collimated arrangement.

Figure 7: *Comparison of transmission factors of a collimated array for 0.662 MeV energy*

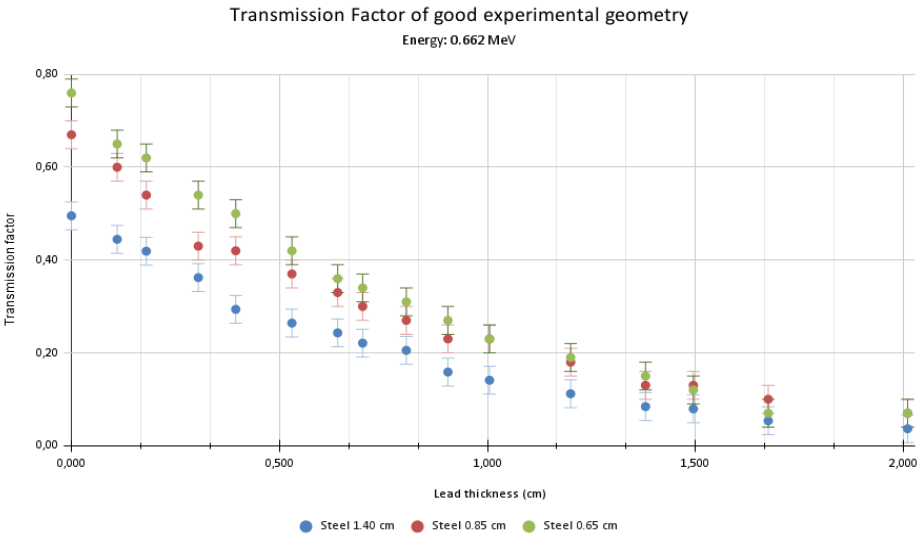

Figure 8: *Comparison of transmission factors of a collimated array for 1.17 MeV energy.*

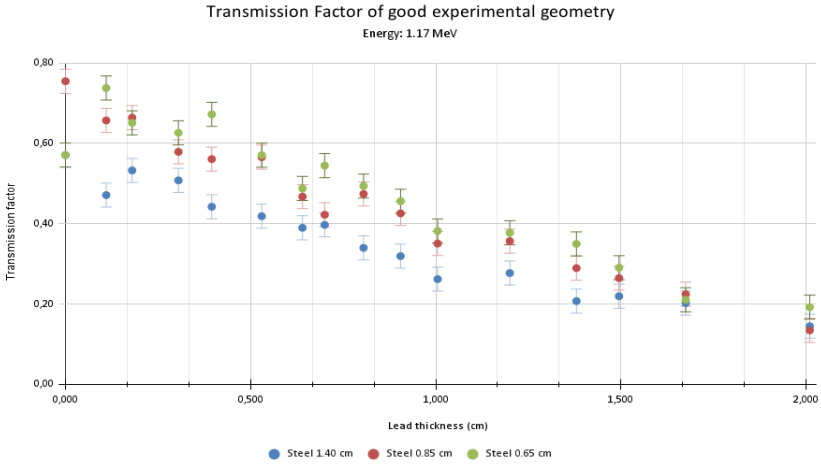

Figure 9: *Comparison of transmission factors of a collimated array for 1.33 MeV energy*

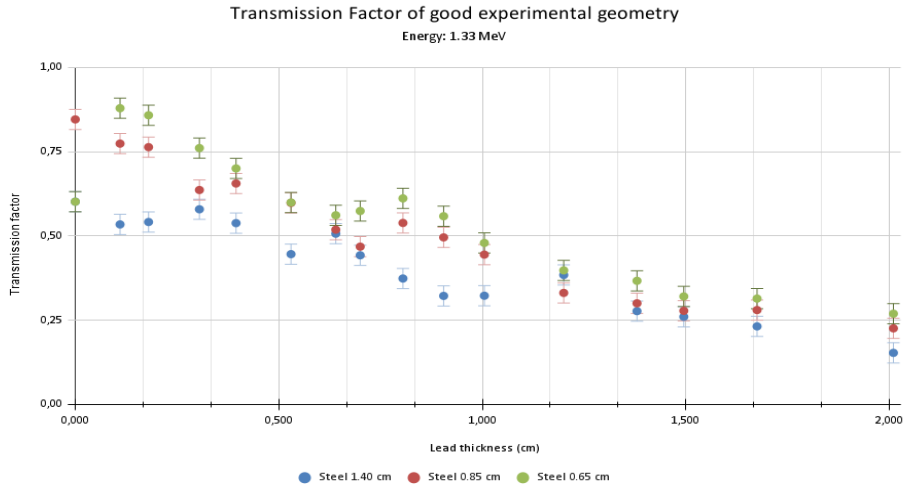

From the analysis of Figure 10, it was verified that there is an occurrence of overlapping of the characteristic emission photopics of Co-60 in all thicknesses, due to the high resolution of the detector (for energy of 0.662 keV, it is less than 14%).

Figure 10: *Cobalt-60 liquid spectrum from 0.65 cm steel thickness and 0 cm lead from good experimental geometry.*

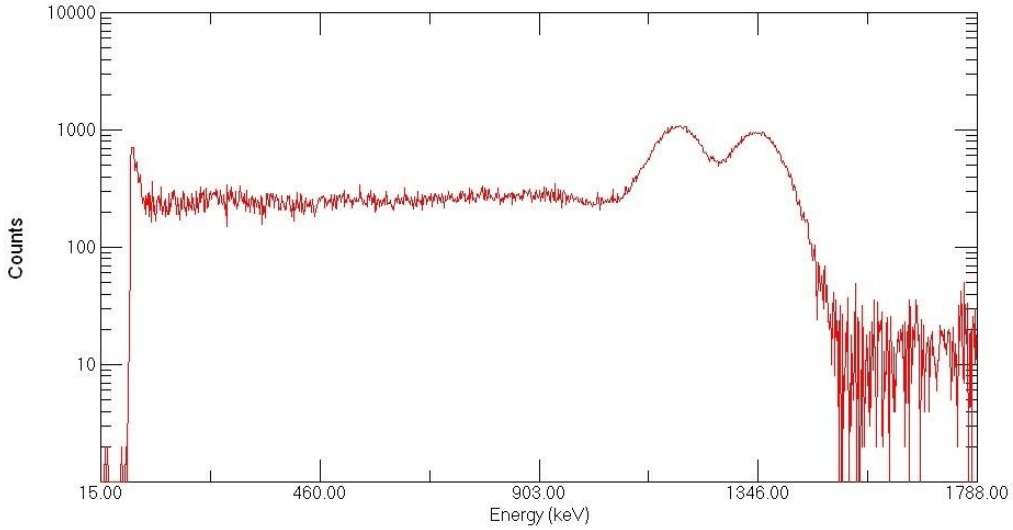

Considering this analysis, it was not possible to better evaluate the results obtained.

Figures 11, 12, and 13 show the results of the transmission factors in the analytical and simulated methodologies, which differed from the experimental results in the lower thicknesses of lead for Cs-137 energy.

Figure 11: *Comparison of transmission factors for 0.662 MeV energy, the thickness of steel 0.65cm*

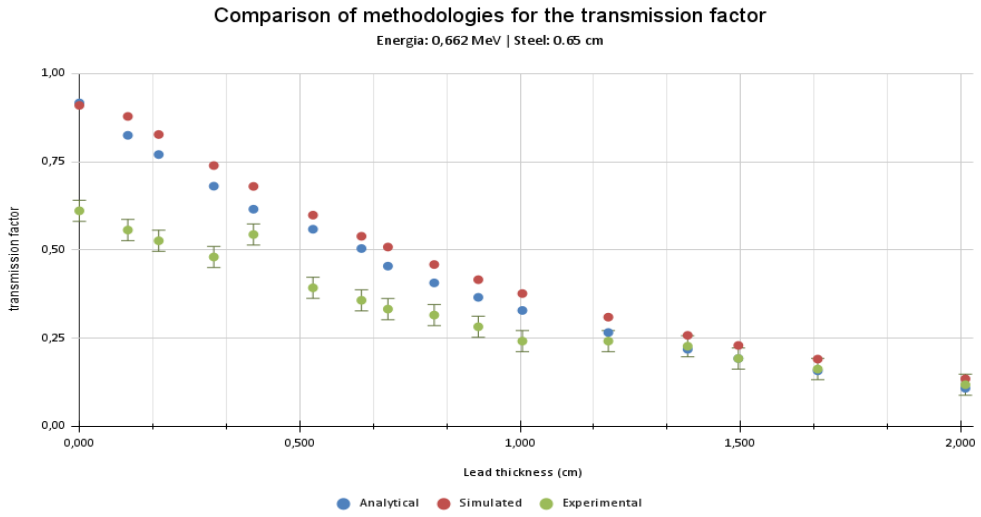

Figure 12: *Comparison of transmission factors for 0.662 MeV energy, the thickness of steel 0.85 cm.*

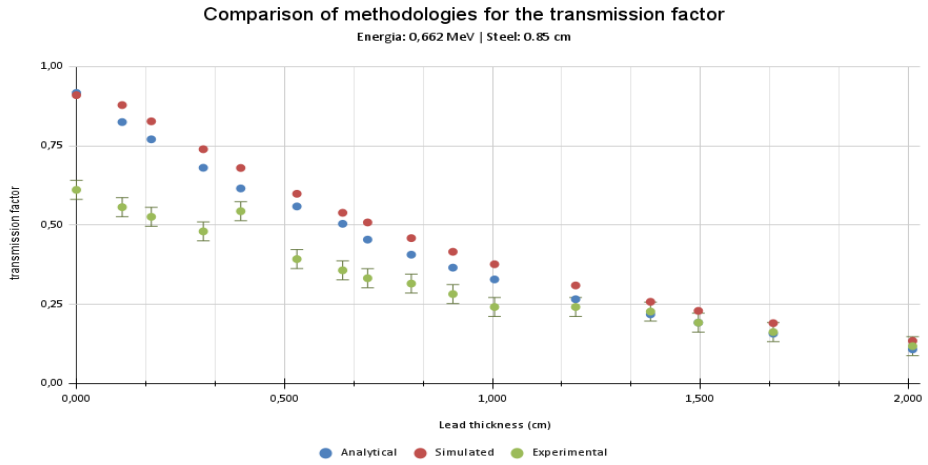

Figure 13: *Comparison of transmission factors for 0.662 MeV energy, the thickness of steel 1.40cm*

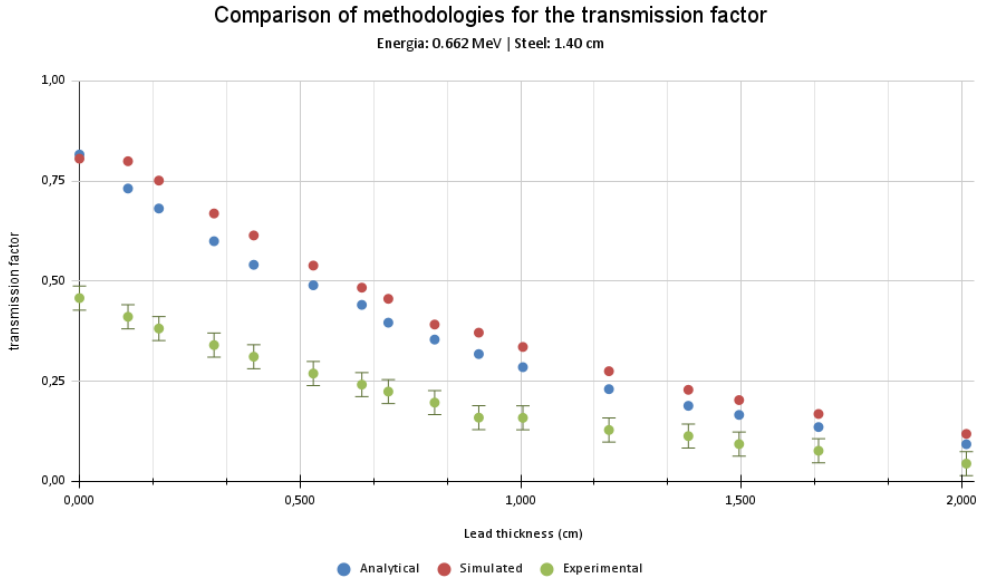

The experimental result is associated with the solid angle of incidence, as shown in Figure 14. One hypothesis for this result is the divergent dimensions of the absorbers.

Figure 14: *Various angles of incidence*

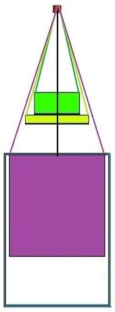

Due to the discrepant results obtained for the Cs-137 energy, measurements were not taken for the Co-60 energies for the non-collimated arrangement. However, the hypothesis of divergent dimensions of the absorbers was investigated through simulation in *MCNP5*.

The non-collimated experimental setup was simulated with the proposed 12x12cm shield dimensions. The thickness chosen was 0.11 cm of lead and 0.65 cm of steel, as it is the minimum bi-laminated shield thickness used in this work.

The simulation was performed both with and without shielding and with 100 million stories (NPS). The simulation sketch is shown in Figure 15.

Figure 15: *Sketch of the experimental apparatus of the non-collimated array with the proposed correction*

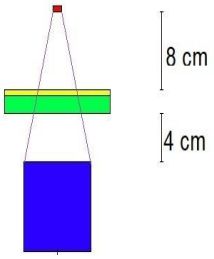

In Figure 15, the source is in red, the lead shielding in yellow, the steel absorber in olive green, and the BGO detector crystal in blue.

The result for the transmission factor of this simulation was 0.83 with uncertainty associated with the measurement less than 0.001.

Comparing the results obtained with the analytical and simulated methodologies, the hypothesis of divergent absorber dimensions can be confirmed, as shown in Table 14.

Table 14: Comparative result of the transmission factor for the energy of 0.662 MeV.

Analytic	Sphere simulation (F1 tally)	Experimental	Experiment simulation
0.84	0.90	0.63	0.83

4.2. Analytical analysis

It was verified that the results of the analytical transmission factor, exponential attenuation, and buildup factor were as expected when compared to the various thicknesses of steel.

Figure 16: *Transmission factors for 0.662 MeV.*

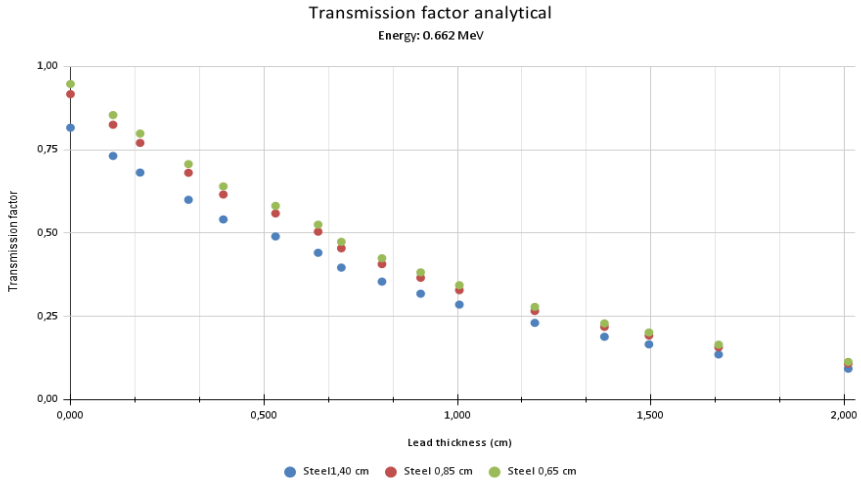

Figure 17: *Transmission factors for 1.17 MeV.*

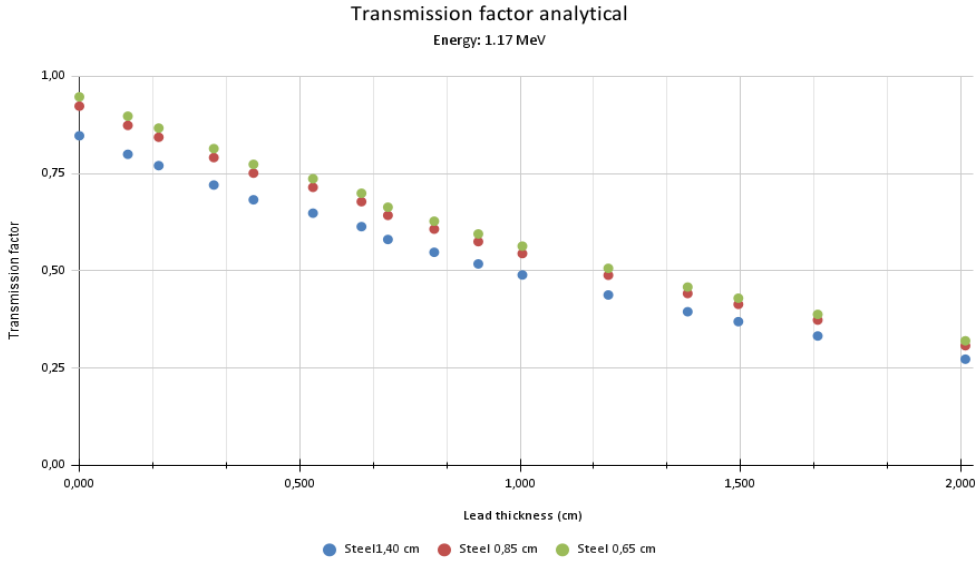

Figure 18: *Transmission factors for 1.33 MeV.*

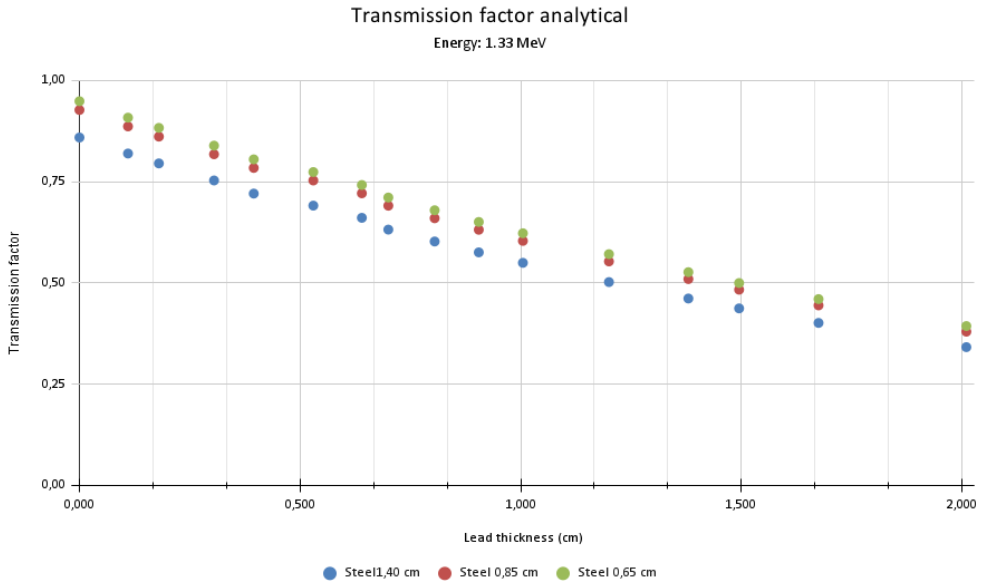

4.3 Simulation analysis

The results of the simulated transmission factor, exponential attenuation, and buildup factor were found to be as expected. It was observed that the responses are similar when compared to the different thicknesses of steel.

Figure 19: *Transmission factors simulated for 0.662 MeV.*

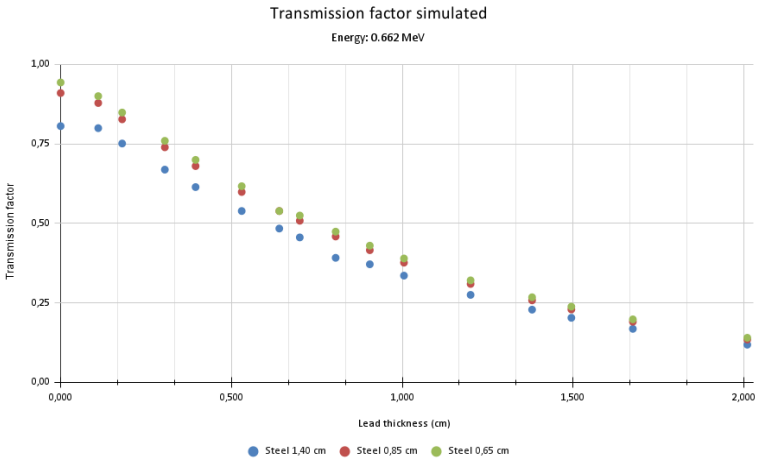

Figure 20: *Transmission factors simulated for 1.17 MeV.*

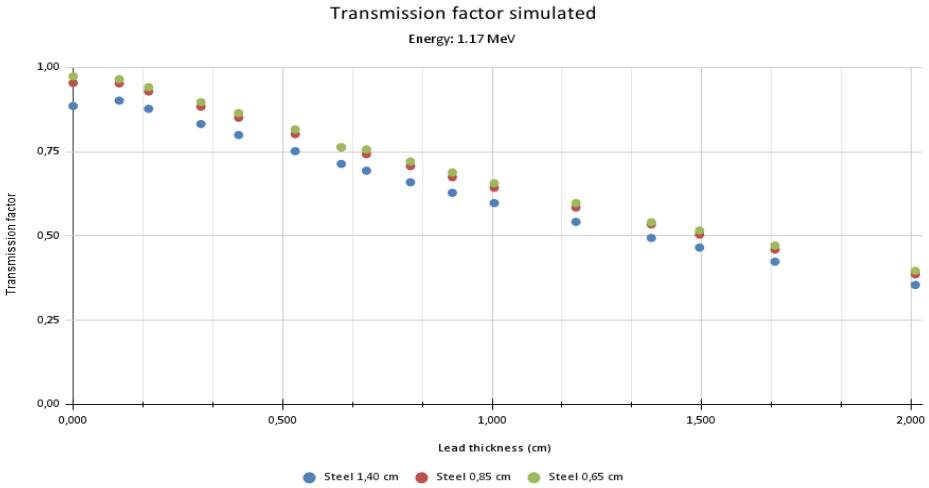

Figure 21: *Transmission factors simulated for 1.33 MeV.*

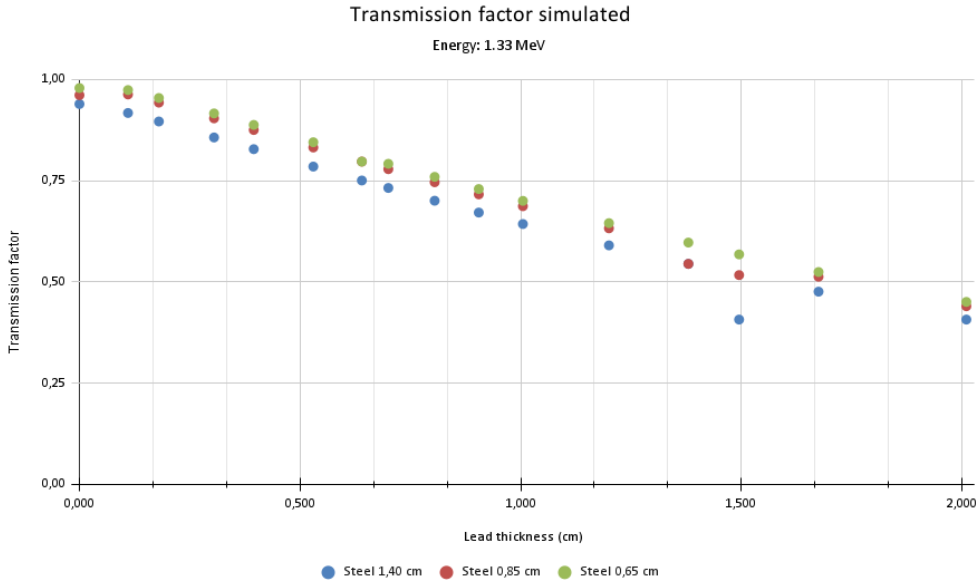

5. CONCLUSIONS

1. The adopted analytical methodology proved to be efficient for calculating the transmission factor of the proposed shielding. It can be considered as a design protocol for bi-laminated steel and lead shielding;

2. The analytical calculations of the transmission factor, buildup factor, and exponential attenuation, when compared to simulated results, respectively, showed compatibility with bilaminated shielding calculations;
3. Due to the low resolution of the BGO detector, the transmission factor curves of the collimated experimental setup for the Cobalt-60 source were inconclusive;
4. Based on the analysis performed in subsection 4.1, it was found that the dimensions of the absorbers (width x length), in the hypothesis of being smaller than the sensitive area of the detector and with divergent sizes, create multiple angles of incidence, generating discrepant data when compared to the proposed methodology.
5. As a suggestion for future works, measurements should be carried out with absorbers of adequate dimensions and with a detector that has resolution capable of showing the formation of Cobalt-60 photopic peaks.

REFERENCES

[1] BRODER, D. L.; KAYURIN, Y. P.; KUTUZOV, A. A. **Transmission of gamma radiation through heterogeneous media**. In: Atomnaya Energlya. [S.l.: s.n.], 1962. pp. 30–35.

[2] HELERBROK, R. " **Chernobyl Accident"**; Brazil School. Access in: Dec. 22.

2021. Available in: <https://brasilescola.uol.com.br/historia/chernobyl-acidente-nuclear.htm>.

[3] GOIÁS, S. of health of. **Cesium 137 Goiânia**. Access in: Dec 22. of 2021. Available in: <https://www.saude.go.gov.br/ cesio137goiania>.

[4] RED, O. M. of the beach. **Conceptual Topics. 2020.** Access in: Dec 22. 2021. Available in: <http://ompv.eceme.eb.mil.br/index.php?option=com_content&view=article&id=165>.

[5] ANGELS, R. R. G. dos. **Evolution of tanks in the Brazilian Army.** 31 p. Monograph (Graduation in Military Sciences) — Academia Militar das Agulhas Negras, Rio de Janeiro, 2019.

[6] BRUNATTO, S. F. **INTRODUCTION TO THE STUDY OF THE ITEMS**. Access in: Apr. 21, 2022. Available in:

http://ftp.demec.ufpr.br/disciplinas/TM052/Prof.Silvio/INTRODU%C3%87%C3%83O%20AO%20ESTUDO%20DOS%20A%C3%87OS-Parte%204.pdf

[7] NUCLEID.ORG. **Library for gamma and alpha emissions**. Access in: Dec. 27, 2021. Available in: <http://www.nucleide.org/Laraweb/index.php>.

[8] STANDARDS, N. I. of; LABORATORY, T. P. M. XCOM: **Photon Cross Sections Database**. Access in: 18 Jun. 2022. Available in: <https://www.nist.gov/pml/xcom-photon-cross-sections-database>.

[9] BRODER, D. L.; KAYURIN, Y. P.; KUTUZOV, A. A. **Calculating gamma buildup factors in heterogeneous media**. In: Atomnaya Energlya. [S.l.: s.n.], 1962. pp. 593–595.

[10] FODERARO, A. **THE FOTON SHIELD MANUAL**. 2. ed. Pennsylvania: The Penn state bookstore, 2014. 344 p.

[11] ATTIX, F. H. **INTRODUCTION TO RADIOLOGICAL PHYSICS AND RADIATION DOSIMETRY.** 3. ed. Wisconsin: Willey-VHC, 1986. 663 p.

[12] SOULFANIDIS, N. **MEASURENT AND DETECTION OF RADIATION**. 4. ed. Boca Raton: CRC Press, 2015. 515p

[13] KOKTA, L. Determination of peak area. Nuclear Instruments and Methods, v. 112, no. 1, p. 245-251, 1973. ISSN 0029-554X. Available at: <https://www.sciencedirect.com/science/article/pii/0029554X73908033>.